Research article

Journal of RAMAN SPECTROSCOPY

Received: 17 September 2012 Revised: 13 December 2012 Accepted: 13 December 2012 Published online in Wiley Online Library: 29 January 2013

(wileyonlinelibrary.com) DOI 10.1002/jrs.4244

Real-time Raman spectroscopy measurements to study the uniaxial tension of isotactic polypropylene: a global overview of microstructural deformation mechanisms

J. Martin,[a,b] M. Ponçot,[b] J.M. Hiver,[b] P. Bourson[a]* and A. Dahoun[b]

ABSTRACT: Micro-Raman spectroscopy was used to investigate the main deformation micromechanisms of isotactic polypropylene uniaxially stretched at constant temperature (T = 30 °C) under a constant true strain rate ($\dot{\varepsilon}_{zz} = 5.10^{-3}\,s^{-1}$). To accurate measurements namely to be free of the recovering phenomenon which causes in most of the cases interference during *post-mortem* analysis, we introduced a new experimental setup combining a Raman spectrometer with a tensile machine piloted by the VidéoTraction™ system. Microstructure is described by essential parameters such as the crystallinity index, the macromolecular orientation both in the crystalline and the amorphous phase, and distribution of the internal stress at the chemical bonds scale. For each, a well-tried Raman spectral criterion was used. Cross-checking of these results, obtained with a minimum of tensile tests, allows a more complete understanding of the deformation micromechanisms of semi-crystalline polymer. Copyright © 2013 John Wiley & Sons, Ltd.

Keywords: polymer; deformation micromechanisms; crystallinity index; macromolecular orientation; *in situ*

Introduction

Macroscopic properties of materials, such as the mechanical behaviour, are closely related to their own microstructures.[1] In the case of semi-crystalline polymers, the crystallinity index and the macromolecular orientation in the crystalline and the amorphous phase are considered to be the essential parameters to understand this relationship and to optimize the end-use properties of such kind of materials.[1–3] At the macroscopic scale, mechanical properties are determined on normalized sample shapes using conventional uniaxial tensile tests.[4] At the microscopic scale, a number of indirect analytical techniques can be used to investigate the microstructure such as thermal analysis, microscopic observations, X-ray scattering, birefringence and nuclear magnetic resonance.[5–7] By collecting both these macroscopic and microscopic data, numerous experimental works have attempted to associate one state of the deformation (such as a strain value) to one state of the microstructure (such as a macromolecular orientation level) in order to propose elementary descriptive models of the deformation micromechanisms.[8–12] A good review of these deformations mechanisms has been published by Bowden and Young.[13] In that vein, the papers of Peterlin[9], focused on polyethylene and polypropylene, developed the first models showing how the crystalline structure are sheared, rotated and fragmented under uniaxial tension. Numerous studies have improved existing models by introducing the metallurgical concept of dislocation and glide systems involving slip within the lamellar crystals during the yielding.[14–16] Contribution of the amorphous phase was then introduced by Treloar *et al.*[17], Young *et al.*[18] and Bartczak *et al.*[19] and then computed by Van der Giessen *et al.*[20] and G'Sell *et al.*[21] by considering a composite approach of the material. Central role of the tie molecules localized inside the amorphous interlamellar layers in the specific stages of viscoelastic and plastic deformation, and then in failure was evidenced in pioneering works by Nitta and Takayanagi.[22,23] However, in many cases, interpretation of these mechanisms is debatable for two major experimental limits. (1) In the case of ductile materials which experience a pronounced necking due to their plastic instability (such as polymers), conventional mechanical tests used widely by the past and giving access to the nominal stress – strain curve are inappropriate to reveal their real mechanical behaviour at prescribed temperature and strain rate.[24,25] In order to perform quantitative measurements, geometry variations in the necking zone of the stretched sample have to be taken into account along the entire course of the tensile test.[26,27] (2) Furthermore, conventional analytical techniques suffer from a common difficulty related to their rather elaborate instrumental setup, often costly and bulky, which requires in most of the cases *post-mortem* analysis and destructive sampling procedure coupled with serious risks of structural damage. For accurate measurements, one has to consider the microstructural evolution in real time with the deformation especially to avoid the material recovering which occurs after sample unloading.[17,28–30] The main purpose of this work is thus to

* *Correspondence to: P. Bourson, Laboratoire Matériaux Optiques, Photonique et Systèmes, Université de Lorraine et Supélec, EA 4423, 2 rue Edouard Belin, 57070 Metz, France. E-mail: bourson@univ-metz.fr*

a *Laboratoire Matériaux Optiques, Photonique et Systèmes, Université de Lorraine et Supélec, EA 4423, 2 rue Edouard Belin, 57070 Metz, France*

b *Institut Jean Lamour, Département SI2M, UMR CNRS 7198, Nancy Université, Parc de Saurupt, 54011 Nancy, France*

Journal of RAMAN SPECTROSCOPY

overcome these two experimental difficulties by coupling two original experimental instruments:

i) On the one hand, by using a video-controlled testing device (called VidéoTraction™), developed in our laboratory by G'Sell and Hiver[31–33], the true constitutive mechanical behaviour of semi-crystalline polymers is determined under a constant true strain rate by taking into account the plastic instability of the polymer which occurs during the deformation.
ii) On the other hand, a Raman spectrometer is coupling to the tensile test machine allowing *in situ* acquisitions. Due to its recent instrumental improvements in particular the advent of laser radiations and the development of couple charge device detectors, Raman spectroscopy is adapted for polymer microstructure characterization with reliability, rapidity and commodity.[34–36] It gives access to the vibrational frequencies of the covalent chemical bonds of polymers and allows analysis of molecular species at different scales, from the chemical repetitive unit to the conformational architecture of the macromolecular chain.[37,38]

In this paper, we propose to apply this experimental setup in a practical application, e.g. to follow the microstructural evolution of an isotactic polypropylene (iPP) in real time with its uniaxial stretching over a large true strain range, from the elastic to the stress hardening deformation domains. Major microstructural features are considered such as the crystallinity index, the macromolecular orientation (both in the crystalline and the amorphous phases) and the internal stress distribution at the chemical bonds scale. On this point, Colomban *et al.*[39,40] reported some valuable *in situ* results performed on polyethylene terephtalate, polyamide 66 and iPP. However, these investigations are only based on the low-wavenumber spectral range of the Raman spectrum (collective modes), and the deformation domain under consideration was limited to the viscoelastic response of the polymers. Moreover, numerous studies relating Raman spectroscopy *in situ* measurements deal with the stress-induced Raman wavenumber shifts[41–44] but only few papers about Raman bands intensity.[45,46]

On the basis of previous elementary descriptive models, our results are principally discussed in terms of deformation micromechanisms which explain the narrow relationship between the polymer mechanical behaviour and its microstructure.

Experimental details

Material

The investigated polypropylene was manufactured by Atochem under the reference 3050 MN1. It is an iPP grade. The weight index of crystallinity, $<X_c>$, is determined by differential scanning calorimetry measurements performed at a heating rate of 10 °C.min^{-1}. Results show a melting point located at $T_m = 165$ °C with an enthalpy of fusion, ΔH_m, equal to 109 J.g^{-1}. This corresponds to a weight index of crystallinity of about 66% (the theoretical enthalpy of fusion considered for a perfect crystal of infinite size, $\Delta H_{t,m}$, is 165 J.g^{-1}).[47,48] The glass transition temperature, T_g, is measured at 5 °C. X-ray scattering measurements evidence the presence of the α-monoclinic form of the iPP crystals. Spherulites of about 55 μm average diameter are observed by means of polarized optical microscopy.

Experimental setup and samples

To follow evolution of the iPP microstructure in real time with its uniaxial deformation, we customized a system coupling a video-controlled tensile machine with a Raman micro-spectrometer. A schematic view of this experimental setup is displayed in a previous paper.[57]The video-controlled mechanical testing method used here the VidéoTraction™ system developed by G'Sell and Hiver.[31] This device provides direct access to the true mechanical behaviour of polymers under uniaxial tension at prescribed temperature, T, and strain rate, $\dot{\varepsilon}_{zz}$, up to very large levels of deformation locally in the neck. Along the entire course of a tensile test, geometry instabilities localized in the necking zone of the polymer sample are taken into account by video measurements. The VideoTraction™ system is widely described in previous papers by G'Sell *et al.*[32,33] and Addiego *et al.*[49]

Raman spectra are collected in backscattered geometry using an iHR250® spectrometer developed by Horiba Jobin Yvon linked to a remote head of probe by means of two optic fibres: one fibre for sending the incident radiation to the sample and the second one for collecting and sending the backscattered radiation to the spectrometer. The head of probe, placed in face to face to the video-controlled system, is equipped with an Olympus long working distance objective lens (× 50 as objective length, × 500 as total magnification, 12 mm as focal distance). Laser radiation coming from a diode laser, producing a λ = 785 nm wavelength radiation, is maintained focused onto the flat surface in the centre of the test sample where necking is expected. At maximum laser power (300 mW), the probe typically delivers an illumination power density of about 15 mW.μm^{-2}. The head of probe is also equipped with a linear polarizer and analyser which allow polarizing the incident laser beam and the Raman scattering radiation, respectively. Rayleigh scattered light is eliminated through a holographic Notch filter placed on the light path just before the diffraction grating (1200 grooves.mm^{-1}). The spectral resolution achieved is about 0.5 cm^{-1}. Previously, the Raman shift is calibrated using a reference sample of pure silicon which shows a well-reported scattering band at 521 cm^{-1}. A micro-computer interfaced with the spectrometer allows recording raw spectra by means of the Labspec® acquisition software (Horiba Jobin Yvon). A self-written fitting least-square procedure based on the Levenberg-Marquardt method is used to process raw data.[50] Residual fluorescence background is eliminated by a polynomial baseline cutting procedure. A mixed Gaussian-Lorentz function is used to decompose each scattering band, and the final adjustment gives access to the useful spectral features such as position, ν (cm^{-1}), integrated intensity, I (a.u) and full width at half maximum (cm^{-1}).

All specimens are stretched at T = 30 °C under a constant true strain rate $\dot{\varepsilon}_{zz} = 5.10^{-3}$ s^{-1} until their rupture at $\varepsilon_{zz} = 1.6$. During the entire course of the tensile test, 40 Raman spectra are recorded. For each Raman spectrum, acquisition time is fixed at 5 s. Note that results are based on the repetition of 10 tensile tests in exactly the same experimental conditions in order to ensure reproducibility.

Measurement procedures

To describe microstructure of iPP under deformation, four microstructural features are considered such as (1) the crystallinity index, (2) the orientation of macromolecules in the crystalline phase, (3) the orientation of macromolecules in the amorphous phase and (4) the distribution of internal stress at the chemical bonds

scale. For each, we adopted a particular Raman spectral criterion developed in our previous study[51–56] on the basis of fundamental works on vibrational mode assignments.[57–61] Table 1 summarized the vibrational mode assignments and the phase belonging (crystalline and/or amorphous) of the Raman scattering bands used to design theses spectral criterions.

The crystallinity index noted $< X_c >$ is deduced from depolarized Raman spectroscopy measurements by determining the criterion $R_c = (I_{809} + I_{842}) / (I_{835} + I_{809} + I_{842})$ of integrated intensity of scattering bands located at 809 (60% crystalline), 835 (0% crystalline) and 842 cm^{-1} (65% crystalline) (Table 1). Due to the fact that bands at 809 and 842 cm^{-1} are not pure crystalline bands, we proposed in a previous study to adjust R_c by balancing factors in order to estimate $< X_c >$ according to the following matching relation:

$$< X_c >= 0.81\ R_c + 0.01 \quad (1)$$

The macromolecular orientation is estimated from Raman spectroscopy by performing measurements in a particular polarization geometry of the incident and scattered radiations noted **x**(**zz**)**x** (as Porto's notation[62]) where both the incident and scattered radiations are polarized along the **z**-stretching direction. In these conditions, we demonstrate in previous papers that the ratio $R_{orient,c} = I_{973} / I_{998}$ of the integrated intensity of the two particular Raman scattering bands at 973 (symmetric stretching mode of the C-C skeletal backbones in crystalline phase) and 998 cm^{-1} (rocking mode of CH_3 lateral alkyl groups in crystalline phase) enable to estimate orientation of crystalline phase chains in the **z**-tensile direction. In uniaxial tension, G'Sell and Dahoun[63] show the development of a fibrillar texture which can be characterized by the determination of only one orientation function, $F_{c/z}$, describing the spatial distribution of the crystallographic **c**-axis towards the **z**-tensile direction. A matching relation between $R_{orient,c}$ and $F_{c/z}$ was established as follow:

$$F_{c/z} = 0.135\ R_{orient,c} - 0.18 \quad (2)$$

Keeping the same polarization configuration, **x**(**zz**)**x**, we used the ratio $R_{orient,am} = I_{835} / I_{tot}$ of the unique band at 835 cm^{-1} (stretching mode of the C-C skeletal backbones in amorphous phase) as a spectral criterion of amorphous chains orientation. I_{tot} is the integrated intensity of the entire recorded spectrum. By the same reasoning, a linear relation was established between $R_{orient,am}$ and orientation function of the amorphous phase $F_{am/z}$ describing the spatial distribution of amorphous macromolecules towards the **z**-tensile direction.

Table 1. Vibrational and phase assignments for Raman scattering bands of iPP [51–61]

Position ν (cm^{-1})	Intensity	Assignment	Phase
809	strong	ν_s(C-C), r(CH2)	Crystalline (60%) Amorphous (40%)
835	medium	ν_s(C-C)	Amorphous
842	strong	r(CH2)	Crystalline (65%) Amorphous (35%)
973	strong	ν_{as}(C-C), r(CH_3)	Crystalline
998	strong	r(CH_3)	Crystalline

$$F_{am/z} = 14.4\ R_{orient,am} - 1 \quad (3)$$

The position dependence of Raman bands *versus* applied stress, commonly called stress-induced Raman shifts, is of fundamental importance in understanding how a macroscopic stress is distributed at the chemical bonds scale.[39–44] These wavenumber shifts are interpreted on the basis of the anharmonicity of chemical bonds, stress inducing an interatomic distance alteration which changes the atomic vibration frequencies.[40] Shifts are expected different according to the nature of the chemical bonds and their orientation towards the macroscopic applied stress direction. A shift towards the low wavenumbers means that bonds are under an extension stress while a shift towards the high ones is related to a compressive stress. In a depolarized configuration, we proposed to follow the normalized shift evolution, $R_s^{809}=\nu_{809}/\nu_{809}^0$, $R_s^{835}=\nu_{835}/\nu_{835}^0$ and $R_s^{842}=\nu_{842}/\nu_{842}^0$ of bands at 809, 835 and 842 cm^{-1} as a function of the true axial strain ε_{zz}. ν_{809}^0 is the reference position of the 809 cm^{-1} band reported for no applied stress. Objective is to explore the evolution of stress distribution both in crystalline (809 and 842 cm^{-1}) and amorphous phase (835 cm^{-1}) during the deformation.

Results

Mechanical behaviour

Uniaxial tension of the iPP was performed at T = 30 °C remaining a constant axial true strain rate $\dot{\varepsilon}_{zz} = 5.10^{-3}\ s^{-1}$. Evolution of the true axial stress – strain curve (σ_{zz} – ε_{zz}) is presented in a previous paper.[56] Three different stages can be enlightened. The first one, $\varepsilon_{zz} = 0 - 0.09$, corresponds to the elasto-viscoelastic behaviour of the iPP. The initial slope of the curve corresponds to the elastic Young's modulus, E = 1.7 GPa. The yield point is defined when stress σ_{zz}^y achieves 36 MPa and passes through a round-off maximum at strain $\varepsilon_{zz}^y = 0.09$. The second stage, $\varepsilon_{zz} = 0.09 - 0.8$, corresponds to the stress-softening regime. At the beginning, stress is marked by a small but significant stress decrease while necking occurs and spreads towards the RVE. This is then followed by a symmetric propagation of the neck shoulders towards the specimen heads at almost constant stress, $\sigma_{zz} = 32$ MPa (easy plastic flow). The last stage, $\varepsilon_{zz} = 0.8 - 1.6$, termed as the plastic stress-hardening regime, shows a nearly exponential increase of the stress from 32 to 71 MPa.

Crystallinity index

Figure 1 shows fitted Raman spectra recorded in the useful spectral range 780 – 860 cm^{-1} at growing true axial strain level, ε_{zz} = 0, 0.1, 0.8 and 1.4. Intensity of bands at 809 and 842 cm^{-1}, which are characteristics of the crystalline phase, decreases regularly with the increasing deformation. On the contrary, intensity of one at 835 cm^{-1}, exclusively associated to the amorphous phase, increases with the increasing deformation. This observation evidences qualitatively a loss of the amount of crystallinity in iPP semi-crystalline microstructure along stretching. Chains initially present in the crystalline phase go through the amorphous one. On the same figure, we note shifts of bands. This point will be discussed further in details. Figure 2 presents evolution of the crystallinity index of iPP, $< X_c >$, *versus* the axial true strain, ε_{zz}. It confirms the general decrease of the crystalline phase amount with the increasing deformation. Evolution marked a three-stage

Journal of RAMAN SPECTROSCOPY

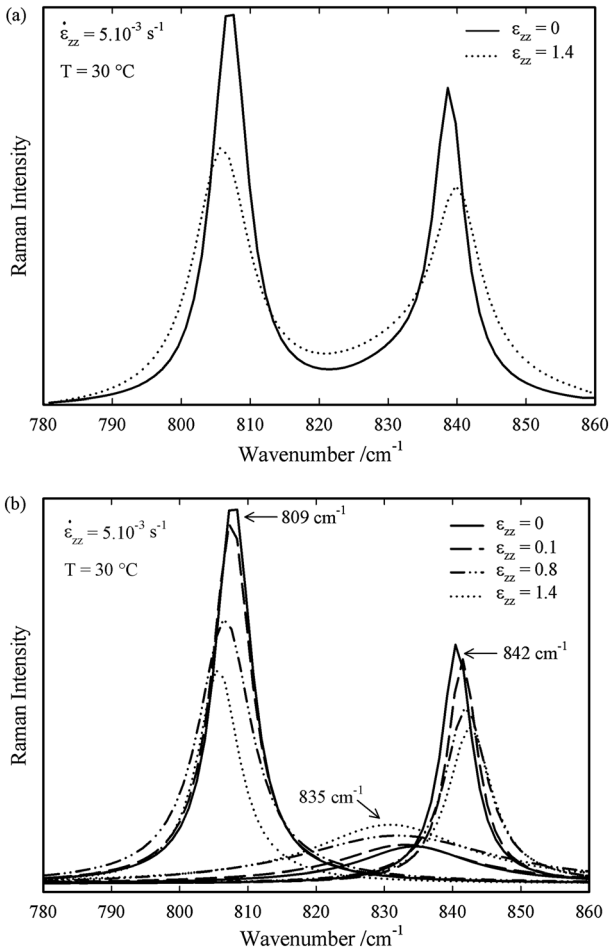

Figure 1. (a) Depolarized Raman spectra and (b) fitted scattering bands at 809, 835 and 842 cm^{-1} of iPP stretched at different strain levels.

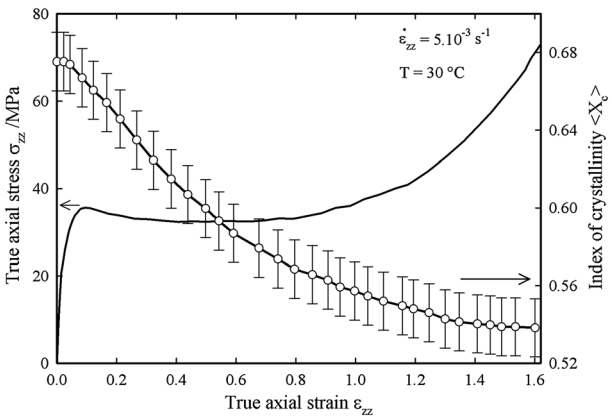

Figure 2. Evolution of the true axial stress, σ_{zz}, and the crystallinity index, $<X_c>$, as a function of the true axial strain, ε_{zz}, of iPP uniaxially stretched at T = 30 °C under a constant true strain rate $\dot{\varepsilon}_{zz} = 5.10^{-3}\ s^{-1}$.

evolution corresponding to the three domains enlightened in the true mechanical behaviour curve: (1) in the elasto-viscoelastic regime, from 0 to 0.09, the crystallinity index is high and quite constant, $<X_c> = 0.67$, (2) then drops drastically in the stress-softening deformation regime, from 0.09 to 0.8, passing from $<X_c> = 0.67$ to 0.57 and (3) finally decreases softly in the stress-hardening regime, from 0.8 to 1.6. Just before rupture, the crystallinity index is low and equal to $<X_c> = 0.54$.

Orientation of macromolecules in the crystalline phase

Figure3 reports fitted Raman spectra recorded in polarized configuration, **x(zz)x**, at growing true axial strain level, $\varepsilon_{zz} = 0$, 0.1, 0.8 and 1.4. The spectral range under consideration, 950 – 1010 cm^{-1}, includes the useful scattering bands at 973 and 998 cm^{-1} required for estimating orientation of chains in the crystalline phase. Intensity of the band at 973 cm^{-1} (symmetric stretching vibration mode of the C-C bond of the skeletal backbones) increases with strain. This corresponds to a larger proportion of C-C skeletal backbones oriented in the **z**-polarization direction parallel to the **z**-stretching axis. Just the opposite is observed for band located at 998 cm^{-1} (rocking vibration mode of the CH_3 lateral alkyl groups) because number of CH_3 lateral groups becomes lower in the **z**-stretching direction. Figure 4 shows the evolution of the orientation function of the crystalline phase, $F_{c/z}$, and the true axial stress σ_{zz} as a function of the true strain ε_{zz} from 0 to 1.6. Increasing evolution of $F_{c/z}$ with deformation is consistent with a gradual orientation of crystalline chains towards the **z**-tensile direction and can be described into three major domains with respect to the true axial strain, ε_{zz}:

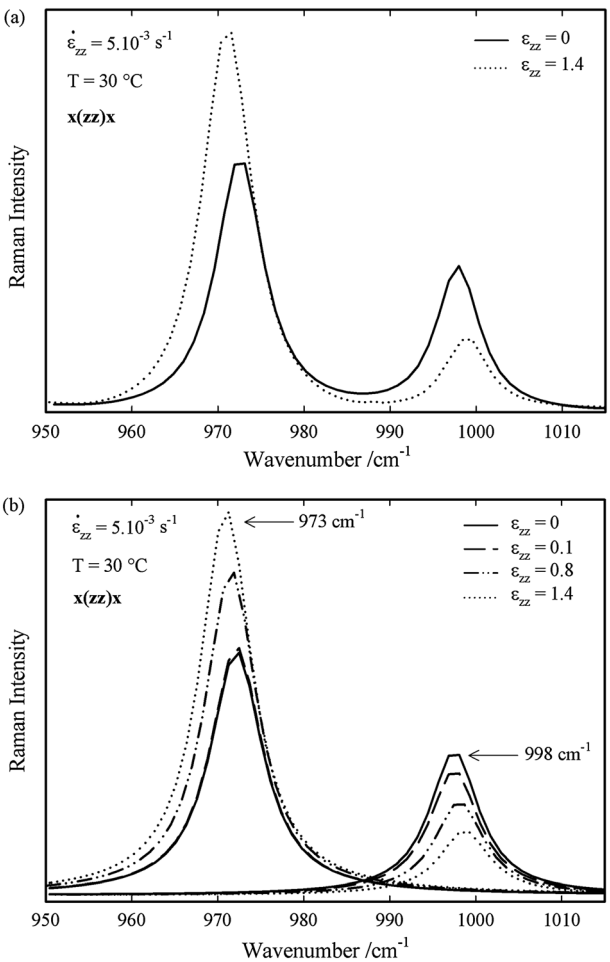

Figure 3. (a) Polarized **x(zz)x** Raman spectra and (b) fitted scattering bands at 973 and 998 cm^{-1} of iPP stretched at different strain levels.

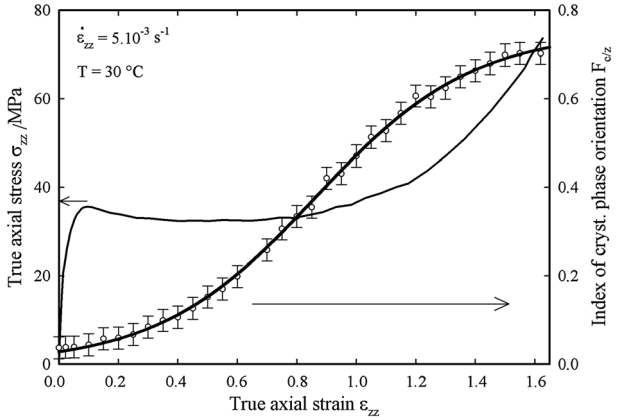

Figure 4. Evolution of the true axial stress, σ_{zz}, and the orientation function of the crystalline phase, $F_{c/z}$, as a function of the true axial strain, ε_{zz}, of iPP uniaxially stretched at T = 30 °C under a constant true strain rate $\dot{\varepsilon}_{zz} = 5.10^{-3}\ s^{-1}$.

i) In the elasto-viscoelastic regime, from 0 to 0.09, $F_{c/z}$ is low and quite constant, $F_{c/z} = 0.05$. It indicates that crystalline chains are still randomly oriented in the material.
ii) In the stress-softening deformation regime, $F_{c/z}$ increases gradually from 0.05 to 0.48. This is related to the beginning of the crystalline chains orientation towards the **z**-tensile direction. We can notice that the inflection point of the increasing evolution of the orientation function is localized at nearly $\varepsilon_{zz} = 0.85$, $F_{c/z} = 0.36$. It suggests that the orientation mechanisms of crystalline chains take a predominant place for this particular strain level.
iii) In the last stress-hardening regime, $F_{c/z}$ is still increasing but its progression becomes milder. Approaching the fracture, $F_{c/z}$ is maximal and quite constant $F_{c/z} = 0.74$ suggesting that crystalline chains have almost achieved their maximal orientation level before the material rupture.

Orientation of macromolecules in the amorphous phase

Figure 5 shows fitted Raman spectra recorded in polarized configuration, **x**(**zz**)**x**, at growing true axial strain level, $\varepsilon_{zz} = 0$, 0.1, 0.8 and 1.4. In the spectral range considered,780 – 880 cm^{-1}, is only plotted the useful polarized scattering band at 835 cm^{-1} which allows calculation of the orientation function of the amorphous chains $F_{am/z}$ taking the **z**-tensile direction as reference. Intensity of this band increases simultaneously with the deformation. This observation is interpreted by considering both the chemical bond associated to this scattering band, e.g. the symmetric stretching mode of the C-C skeletal backbones in the amorphous state and the polarization direction. An increasing intensity evidences an increase of C-C bond proportion oriented parallel to the **z**-polarization direction which is also the stretching direction. Thus, chains of amorphous phase tend to be preferentially oriented along the **z**-tensile direction. Figure 6 presents the evolution of the orientation function of the amorphous phase $F_{am/z}$, and the true axial stress σ_{zz} as a function of the true strain ε_{zz} from 0 to 1.6. Increasing evolution of $F_{am/z}$ with deformation confirms our preliminary observations: macromolecular chains tend to be oriented towards the **z**-tensile direction. It can be delimited with respect to the true axial strain, ε_{zz}: (1) in the elasto-viscoelastic regime, from 0 to 0.09, chains are profoundly affected by the deformation since $F_{am/z}$ raises from 0.03 to 0.3; (2) in the stress-softening regime, from 0.09 to 0.8, orientation of amorphous is milder passing from $F_{am/z} = 0.3$ to 0.6 and (3) becomes more and more moderate $F_{am/z} = 0.6$ – 0.7 in the stress-hardening regime, from 0.8 to 1.6. Approaching the fracture deformation, $F_{am/z}$ exhibits a maximal and quite constant value, $F_{am/z} = 0.7$, suggesting that amorphous chains have almost achieved their maximal orientation level before rupture.

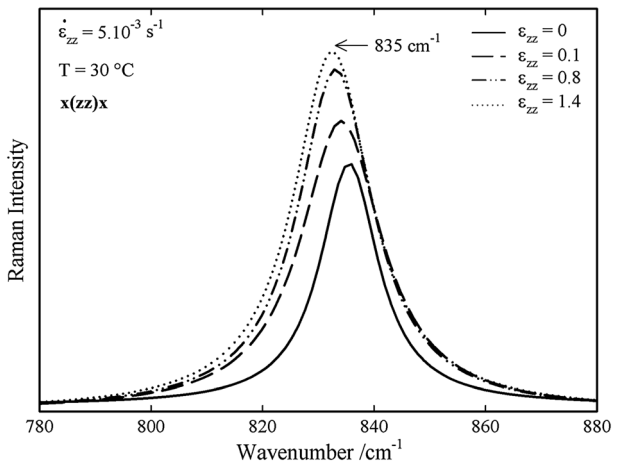

Figure 5. Fitted Raman scattering band at 835 cm^{-1} for different strain levels of iPP recorded in the **x(zz)x** polarized light configuration.

Stress distribution

In Figs. 1 and 3, we have noted that bands at 809, 835 and 841 cm^{-1} exhibit opposite wavenumber shifts with deformation. Bands at 809 and 835 cm^{-1} possessing both a high contribution of the C-C skeletal backbones move towards low wavenumbers. This indicates that these chemical bonds experience an increasing extension stress with the increasing deformation as described by. On the contrary, crystalline band at 842 cm^{-1}, principally attributed to the CH_2 lateral groups, moves up to high wavenumbers. This evidences the compressive solicitation that endures C-H lateral bonds during stretching. These observations are in good agreement with previous studies of Wool *et al.* [64] in case of polyethylene. Figure 7 shows evolution of the normalized position, ν/ν^0 of the crystalline bands at 809 and 842 cm^{-1} whereas Fig. 8 plots the amorphous one at 835 cm^{-1}. ν^0 represents position

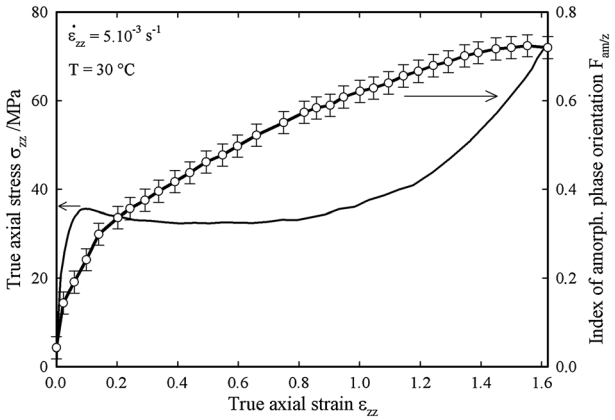

Figure 6. Evolution of the true axial stress, σ_{zz}, and the orientation function of the amorphous phase, $F_{am/z}$, as a function of the true axial strain, ε_{zz}, of iPP uniaxially stretched at T = 30 °C under a constant true strain rate $\dot{\varepsilon}_{zz} = 5.10^{-3}\ s^{-1}$.

Journal of RAMAN SPECTROSCOPY

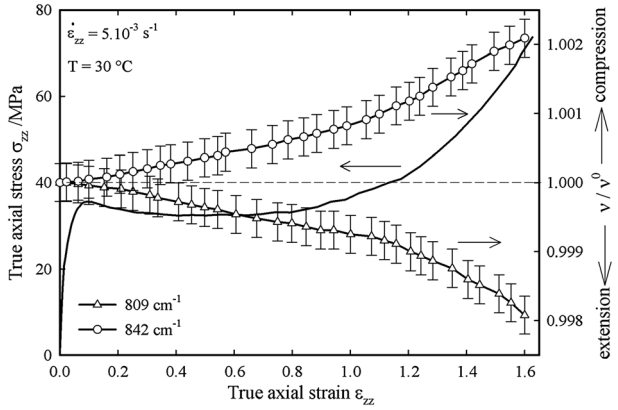

Figure 7. Evolution of the true axial stress, σ_{zz}, and the normalized position, ν / ν^0, of crystalline bands at 809 (C-C) and 842 cm^{-1} (CH_2).

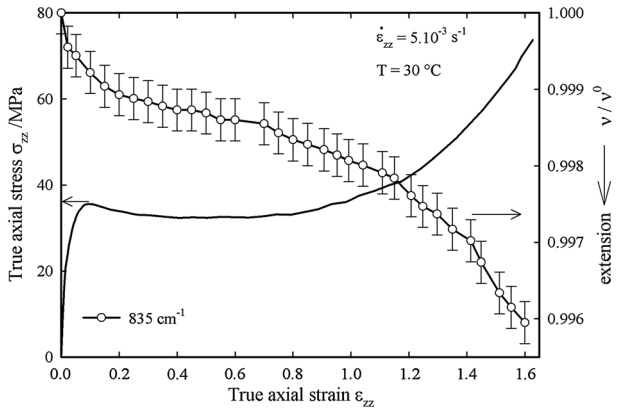

Figure 8. Evolution of the true axial stress, σ_{zz}, and the normalized position, ν / ν^0, of amorphous band at 835 cm^{-1} (C-C) as a function of the true axial strain, ε_{zz}, of iPP uniaxially stretched at T = 30 °C under a constant true strain rate $\dot{\varepsilon}_{zz} = 5.10^{-3}\ s^{-1}$.

of bands for the non-deformed iPP. Despite that shift of crystalline bands at 809 and 842 cm^{-1} have an opposite behaviour, their evolutions are comparable as a function of the true axial strain, ε_{zz}:

i) In the elasto-viscoelastic regime, from 0 to 0.09, normalized shifts of both bands are very low. This indicates that application of extension stress on the C-C skeletal backbones and compressive stress on C-H lateral bonds is weak as if crystalline chains are not yet regarded by the deformation.
ii) In the stress-softening regime, from 0.09 to 0.8, positions of bands move gently meaning that stress is progressively applied on chemicals bonds.
iii) In the last stress-hardening regime, from 0.8 to 1.6, bonds are strongly constrained since shifts exhibit important variations.

By comparing evolution of the extension stress on C-C bonds between crystalline (Fig. 7) and amorphous chains (Fig. 8), we note major differences particularly in the elasto-viscoelastic regime where amorphous C-C bonds are highly constrained while crystalline ones are not yet affected.

Discussion

Discussion focuses on the description of the deformation micromechanisms occurring in the semi-crystalline structure of iPP by clearly discerning the three different regimes of the true mechanical behaviour: (1) the elasto-viscoelastic regime, (2) the stress-softening regime and (3) stress-hardening regime. Discussion is based on the cross-checking of the results obtained previously and summarized in Table 2. Such a rigorous description has to take into account two special crystal features of the α-iPP spherulites: (1) the high dependence of the initial orientation of lamellae, distributed in equatorial, diagonal and polar regions of the spherulite, with respect to the macroscopic applied stress **z**-direction[65]; (2) the cross-hatch type lamellar branching which exhibits radial ('mother') and tangential ('daughter') lamellae nearly oriented orthogonally one to the other.[48] Radial lamellae correspond to the $\mathbf{c_1}$-crystallographic axis and the tangential ones to the $\mathbf{c_2}$-axis. This last point explains strongly the mechanical behaviour differences observed with the β-iPP spherulites which consist of broad, locally stacked radial lamellae, just as in spherulites of polyethylene.[66,67] Under tensile loading, it has been shown that the α-iPP spherulites exhibit brittle behaviour whereas the β-ones deform plastically with little damage (occurrence of cavitation) up to strain of about $\varepsilon_{zz} = 0.25$.

Elasto-viscoelastic regime

In the elasto-viscoelastic regime (Fig. 9), $\varepsilon_{zz} = 0 - 0.09$, results demonstrate that it is only the amorphous phase which plays a major role in the deformation process: orientation of amorphous chains is high and accompanied by the application of an important extension-stress level on the amorphous C-C skeletal backbones. On the contrary, deformation mechanisms involving crystalline phase are not yet active: neither the crystalline chains orientation nor the

Table 2. Raman spectroscopy results on major microstructural aspects of iPP uniaxially stretched at T = 30 °C under a constant true strain rate $\dot{\varepsilon}_{zz} = 5.10^{-3}\ s^{-1}$ from the elastic to the stress-hardening regime

Microstructural aspect	Descriptive parameter	Deformation regime		
		Elasto-viscoelastic regime	**Stress-softening regime**	**Stress-hardening regime**
		0.00 – 0.09	**0.09 – 0.80**	**0.80 – 1.60**
Crystallinity index	$\langle X_c \rangle$	0.67 – 0.67	0.67 – 0.57	0.57 – 0.54
Crystalline phaseorientation	$F_{C/Z}$	0.05 – 0.05	0.05 – 0.48	0.48 – 0.74
Amorphous phaseorientation	$F_{am/Z}$	0.03 – 0.30	0.30 – 0.60	0.60 – 0.70
Stress on C-C cryst.bonds	ν_{809}/ν^0_{809}	1.0000 – 1.0000	1.0000 – 0.9995	0.9995 – 0.9980
Stress on C-C amor. bonds	ν_{835}/ν^0_{835}	1.0000 – 0.9990	0.9990 – 0.9985	0.9985 – 0.9960
Stress on C-H cryst. bonds	ν_{842}/ν^0_{842}	1.0000 – 1.0000	1.0000 – 1.0005	1.0005 – 1.0020

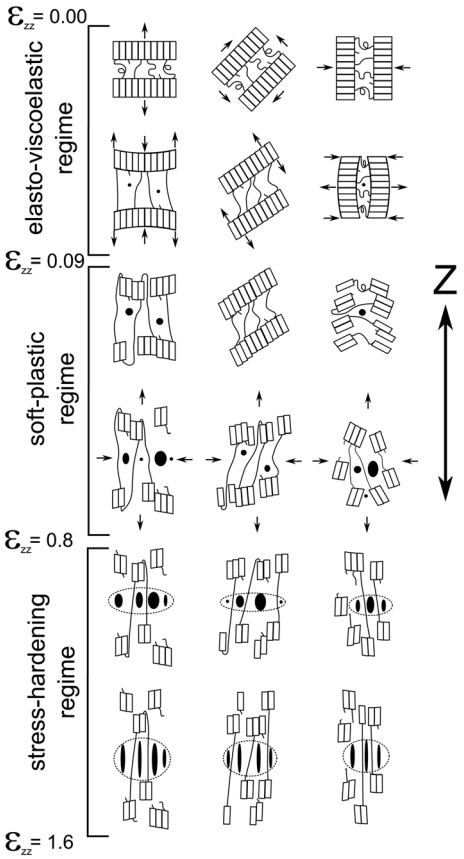

Figure 9. A schematic illustration of micro-structural mechanisms occurring in uniaxially stretched iPP during the initial elasto-viscoelastic regime, the stress-softening deformation regime and the stress-hardening regime.

crystallinity index changes. This is usually explained by considering the soft amorphous phase behaviour compared with the rigid crystalline blocks. In the analogous case of polyethylene, Schultz *et al.*[10] show that the nanoscopic elastic modulus of one chain is 16 times higher than the macroscopic one evidencing the essential contribution of the soft amorphous phase. For $T > T_g$, the Van der Waals interactions are overcome, and the amorphous part exhibits a rubber-like behaviour. Initially, under an interpenetrating coils configuration, chains in the interlamellar layers have enough macromolecular mobility to orient themselves towards the **z**-tensile direction in order to accommodate the deformation. It involves disentanglement, extension and alignment of the tie molecules between two adjacent crystalline lamellae. This is particularly verified for stacked lamellae oriented perpendicularly to the stretching direction such as for the radial and the tangential ones in the equatorial and the polar regions, respectively. Adjacent lamellae are separated, and the average length of the amorphous interlamellar layer increases.[13] The important extension stress measured on the amorphous C-C skeletal backbones is in good agreement with this interpretation. On the contrary, lamellae in polar regions undergo locally a compressive stress leading to move lamellae closer. Amorphous chains are confined in the interlamellar layer. Radial and tangential lamellae in diagonal regions, inclined at $\pm$ 45 ° with respect to the macroscopic**z**-tensile direction, are locally subject to a shear stress which promotes lamellae sliding. This leads to a progressive extension and alignment of amorphous chains. Deformation of amorphous phase is always at least partially reversible in the elastic domain and time-dependent in the viscoelastic one.[17,18] This is due to the thermodynamic tendency of the stretched chains to return to their coiled geometry.

Stress-softening regime

In the stress-softening regime (Fig. 9), $\varepsilon_{zz} = 0.09 - 0.8$, results show that orientation of the crystalline chains towards the **z**-tensile direction is dominant, the crystallinity index drops drastically, the macroscopic stress is more and more disseminated on the chemical bonds of the crystalline macromolecules and the volume damage is activated. These important changes noted for the crystalline phase signal clearly the activation of new deformation mechanisms differing from these encountered during the viscoelastic regime. After a critical stress is achieved corresponding to the yield point, amorphous phase cannot accommodate any more the increasing deformation because interlamellar extension and/or shearing process is limited by the finite extensibility of the highly entangled chains (or tie molecules). Therefore, these are crystals which are affected at their turn by dissipative deformation mechanisms as plastic flow and formation of micro-voids in the amorphous layers and / or at inter-spherulitic boundaries.[13] In the true stress – strain curve of iPP, the stress drop occurring just past the yield point is caused by the catastrophic and cooperative failures of the lamellae accompanying deformation. In the equatorial regions, Nitta and Takayanagi[22,23] proposed that the tie molecules linking two adjacent lamellae through the interlamellar amorphous zone support the external force and induce a local concentrated load at the lamellae surfaces leading to bending, as shown in Fig. 9. Moreover, the same authors show that under a critical bending stress value, calculating as a function of the tie molecules fraction, lamellae are broken up into smaller blocks. In parallel, our results on crystallinity show that a part of crystalline chains is pulled-out from the folded-chains lamellae. This is commonly termed as the mechanically induced melting process. At the same time, micro-crazes appear in the amorphous layers perpendicularly oriented to the stress direction, and they progressively transform themselves into cavities with the increasing deformation.[12] In the polar regions, the existence of a local compressive stress induces also a lamellar bending in the meaning of Nitta and Takayanagi.[22,23] Crystal blocks are at first pulled out of the lamellae, then rotate towards the z-tensile axis and are subject in part to destruction.[10] Deformation mechanisms in diagonal regions are quite different since radial and tangential lamellae are oriented at $\pm$ 45 ° *versus* the **z**-tensile axis which promotes fine crystallographic slips by generation and glide of dislocations leaving the lamellae intact.[15,16] In uniaxially stretched iPP, it was demonstrated that minimum value of the critical resolved shear stress is first achieved for chain slip mode along the (100)[001], (010)[001], (110) [001] and (1 10)[001] glide systems.[63] For further deformation, this crystal plasticity, that readily accommodates most of the applied deformation, leads to consecutives secondary effects such as (1) plastic tilt of crystallites towards the **z**-tensile axis, (2) lamellae fragmentation owing to coarse slip process, (3) crystalline phase destruction by chains pull-out process and (4) micro-voids formation in the amorphous layers.[8–13] On this last point, it is worth to note that voiding appears earlier in the equatorial and polar regions of the spherulites where plastic slip is less favourable compared to the diagonal ones. These interpretations were assessed by previous microscopy studies on the transition from yielding to crazing in polypropylene concluding to a competition between crystal slip and voiding in governing the propagation of cavitation across the spherulite.[68] In addition, the fact that voids occur at the same time in the

equatorial and polar regions is related to the cross-hatched structure of the α-iPP spherulites and gives credit to the assumption that radial lamellae in equatorial position deformed similarly as the tangential ones in the polar regions and *vice versa*. In the case of polyethylene and polybutene which present both only radial lamellae, Addiego *et al.*[49] and Weynant *et al.*[69] show, respectively, that the structural damage occurs first in the equatorial regions and long after in the polar ones.

Strain hardening regime

In the last strain-hardening domain (Fig. 9), $\varepsilon_{zz} = 0.8 - 1.6$, results show principally that deformation mechanisms involving crystalline and amorphous phase become stable: orientation of the crystalline and amorphous chains is less active, the loss of crystallinity slow down and volume strain achieves practically its maximum level. This means that mechanisms of plastic deformation are depleted, and the initial isotropic lamellar structure is transformed into a highly anisotropic and damaged micro-fibrillar structure oriented towards the tensile direction.[13] Contrary to the stress-softening regime, deformation mechanisms in the strain-hardening one are quite identical in the equatorial, diagonal and polar regions of the α-iPP spherulite as illustrated in Fig. 9. The microstructure accommodates the continuing deformation only by the extension and the valence angle opening of the chemical bonds. The force required for displacing the C-C bonds from their equilibrium distance (related to the Morse's potential) is such important that the stress increases drastically in this last deformation regime. Our results showing important variations of the local stresses at the chemical bonds assesses this interpretation: C-C skeletal backbones of both the crystalline and amorphous macromolecules are more and more under extension since they are oriented in the tensile direction. In contrast, the C-H lateral bonds are more and more compressed since they are practically oriented towards the compressive direction of the uniaxial stress tensor. At large deformations, the ellipsoidal geometry of the voids observed in numerous microscopy studies is directly related to the application of a dilatation and a compaction stress (hydrostatic stress) along the axial and transversal directions, respectively. Approaching the polymer probe failure, crystalline and amorphous chains have achieved their maximal orientation level, the proportion of crystalline phase is low and degraded in favour of the amorphous one and microstructure is highly damaged by the generation of crazes resulting from the nucleation, growth and coalescence of micro-voids (cavity). When chemical bonds cannot support the applied stress anymore, rupture of the polymer occurs by the rapid propagation of a crack (having a critical size) breaking craze fibrils as it grows.[70]

Conclusion

The deformation mechanisms of iPP during its uniaxial tension are investigated at the macroscopic scale by means of a 2D video extensometer (VidéoTraction™) giving access to the intrinsic stress – strain curve of the polymer for a constant true strain rate at constant temperature, and at the microscopic scale by micro-Raman spectroscopy. The new combination of these both analysis techniques is introduced in this work and allows to characterize the polymer microstructure in real time with its deformation by being free of the microstructure relaxation widely observed during *post-mortem* analysis. By this means, we demonstrate that rapidity of the spectral acquisitions presents a particular advantage in performing time-resolved measurements such as the 'step by step' following of the deformation micromechanisms. On the basis of the use of simple but reliable (previously validated) Raman spectral criterions appropriated for crucial features of the iPP microstructure (crystallinity index, chains orientation of both amorphous and crystalline phase and volume strain), we describe evolution of the iPP microstructure in a large deformation domain from its elastic response to its rupture. Deformation of the spherulite microstructure results from a number of mechanisms involving both amorphous and crystalline phase. Such mechanisms are highly dependent on the orientation of structural elements with respect to the stress axis (equatorial, diagonal and polar regions). Results evidence clearly the transformation of the initial isotropic lamellar structure into a highly anisotropic and damaged micro-fibrillar structure oriented towards the stress direction. The main results show:

- The major role played by the amorphous phase during the initial elasto-viscoelastic deformation regime leading to interlamellar and / or shearing mechanisms.
- The major role played by the crystalline phase during the stress-softening deformation regime such as crystal plasticity (for diagonal regions), lamellae destruction owing to a chains pulling-out mechanism, crystal tilting towards the stress direction, fragmentation and voids generation,
- The major role played by the chemical bonds in resisting to the deformation during the last strain-hardening regime.

Further works should be devoted to a closer examination of the amorphous and crystalline phase evolution during loading and unloading cycles in order to have a better understanding of structural mechanisms occurring at the time of the relaxation/recovering of the material microstructure.

References

[1] I. M. Ward, Mechanical Properties of Solid Polymers, Wiley-Interscience, London, **1971**.
[2] R. J. Samuels, Structured Polymer Properties: The Identification, Interpretation, and Application of Crystalline Polymer Structure, John Wiley & Sons, New York, **1974**.
[3] R. J. Young, P. A. Lovell, Introduction to Polymers, Chapman & Hall, New York, **1981**.
[4] C. G'Sell, in Plastic Deformation of Amorphous and Semi Crystalline Materials, (Eds: B. Escaig, C. G'Sell), Les Editions de Physique, Les Ullis, **1990**, pp. 13–25.
[5] B. Wunderlich, Macromolecular Physics: Crystal Structure, Morphology, Defects, Academic Press, New York, **1973a**.
[6] U. W. Gedde, Polymer Physics, Kluwer Academic Publishers, Dordrecht, **1995**.
[7] A. J. de Vries, in Plastic Deformation of Amorphous and Semi Crystalline Materials, (Eds: B. Escaig, C. G'Sell), Les Editions de Physique, Les Ullis, **1982**, pp. 329–344.
[8] I. L. Hay, *Kolloid ZuZ Polym. Band* **1965**, *204*, 43–47.
[9] A. Peterlin, *J. Mater. Sci.* **1971**, *6*, 490–508.
[10] J. Schultz, Polymer Materials Science, Printice-Hall, Englewood Cliffs, **1974**.
[11] J. Petermann, W. Kluge, H. Gleiter, *J. Polym. Sci.* **1979**, *17*, 1043.
[12] K. Friedriech, in Advances in Polymer Science, Crazing in Polymers 52/53, (Eds: H. H. Kausch), Springer-Verlag, Berlin-Heidelberg, **1983**.
[13] P. B. Bowden, R. J. Young, *J. Mater. Sci.* **1974**, *9*, 2034–2051.
[14] H. Gleiter, A. S. Argon, *Philos. Mag.* **1971**, *24*, 71.
[15] A. Keller, D. P. Pope, *J. Mater. Sci.* **1971**, *6*, 453–478.
[16] L. Lin, A. S. Argon, *J. Mater. Sci.* **1994**, *29*, 294–323.
[17] L. R. G. Treloar, The Physics of Rubber Elasticity, Clarendon, Oxford, **1975**.
[18] R. J. Young, P. B. Bowden, J. M. Ritchie, J. G. Rider, *J. Mater. Sci.* **1973**, *8*, 23–26.
[19] Z. Bartczak, A. Galeski, A. S. Argon, R. E. Cohen, *Polymer* **1996**, *37*, 2113–2123.

[20] P. D. Wu, E. Van der Giessen, *Mech. Res. Comm.* **1992**, *19*, 427–433.
[21] C. G'Sell, A. Dahoun, *Mater. Sci. Eng.* **1994**, *175*, 183–199.
[22] K. H. Nitta, M. Takayanagi, *J. Polym. Sci.* **1999**, *37*, 357–368.
[23] K. H. Nitta, M. Takayanagi, *J. Polym. Sci.* **2000** *38*, 1037–1044.
[24] C. G'Sell, in Plastic Deformation of Amorphous and Semi Crystalline Materials, (Eds: B. Escaig, C. G'Sell), Les Editions de Physique, Les Ullis, **1982**, pp. 375–389.
[25] M. Ponçot, F. Addiego, A. Dahoun, *Int. J. Plasticity* **2013**, *40*, 126–139.
[26] C. G'Sell, J. J. Jonas, *J. Mater. Sci.* **1979**, *14*, 583–591.
[27] C. G'Sell, N. A. Aly-Hellah, J. J. Jonas, *J. Mater. Sci.* **1983**, *18*, 1731–1742.
[28] R. H. Boyd, *Polymer* **1985**, *26*, 323–347.
[29] C. Jourdan, J. Y. Cavaille, J. Perez, *J. Polym. Sci.* **1989**, *27*, 2361–2384.
[30] B. Escaig, in Plastic Deformation of Amorphous and Semi Crystalline Materials, (Eds: B. Escaig, C. G'Sell), Les Editions de Physique, Les Ullis, **1982**, pp. 187–225.
[31] C. G'Sell, J. M. Hiver, French Patent #010542100, Bull. Off. INPI, 23 April: **2001**.
[32] C. G'Sell, J. M. Hiver, A. Dahoun, A. Souahi, *J. Mater. Sci.* **1992**, *27*, 5031–5039.
[33] C. G'Sell, J. M. Hiver, A. Dahoun, *Int. J. Solids Struct.* **2002**, *39*, 3857–3872.
[34] D. L. Gerrard, W. F. Maddams, *Appl. Spectrosc. Rev.* **1986**, *22*, 251–334.
[35] S. J. Spells, Characterization of Solid Polymers: New Techniques and Developments, Chapman & Hall, London, **1994**.
[36] G. Xue, *Prog. Polym. Sci.* **1994**, *19*, 317–388.
[37] J. L. Koenig, Spectroscopy of Polymers, Elsevier Science, New York, **1999**.
[38] D. I. Bower, W. F. Maddams, The Vibrational Spectroscopy of Polymers, Cambridge University Press, Cambridge, **1989**.
[39] P. Colomban, J. M. Herrera Ramirez, R. Paquin, A. Marcellan, A. Bunsell, *Eng. Fract. Mech.* **2006**, *73*, 2463–2475.
[40] P. Colomban, *Compos. Sci. Tech.* **2009**, *69*, 1437–1441.
[41] C. Galiotis, *Mater. Technol.* **1993**, *8*, 203–209.
[42] P. J. Hendra, W.F. Maddams, in Polymer Spectroscopy, (Eds: A. H. Fawcett), John Wiley & Sons, Chichester, **1996**.
[43] J. C. Rodriguez-Cabello, J. C. Merino, J. M. Pastor, *J. Raman Spectrosc.* **1996**, *27*, 463–467.
[44] R. J. Young, S. J. Eichorn, *Polymer* **2007**, *48*, 2–18.
[45] J. Purvis, D. I. Bower, *J. Polym. Sci.* **1976**, *14*, 1461–1484.
[46] M. Tanaka, R. J. Young, *J. Mater. Sci.* **2006**, *41*, 963–991.
[47] B. Wunderlich, Macromolecular Physics: Crystal structure, Morphology, Defects, Academic Press, New York, **1973b**.
[48] B. Lotz, J. C. Wittman, *J. Polym. Sci.* **1986**, *24*, 1541–1558.
[49] F. Addiego, A. Dahoun, C. G'Sell, J. M. Hiver, *Polymer* **2006**, *47*, 4387–4399.
[50] K. Levenberg, *Quart. Appl. Math.* **1944**, *2*, 164–168.
[51] J. Martin, Ph. D. Thesis, Université Paul Verlaine, Metz, **2009**.
[52] M. Ponçot, Ph. D., Thesis, Institut National Polytechnique de Lorraine, Nancy, **2009**.
[53] J. Martin, S. Margueron, M. Fontana, M. Cochez, P. Bourson, *Polym. Eng. Sci.* **2010**, *50*, 138–143.
[54] J. Martin, P. Bourson, A. Dahoun, J. M. Hiver, *Appl. Spectrosc.* **2009**, *63*, 1377–1381.
[55] M. Ponçot, J. Martin, J. M. Hiver, D. Verchère, A. Dahoun, *J. Appl. Polym. Sci.* **2012**, *125*, 3385–3395.
[56] J. Martin, M. Ponçot, P. Bourson, A. Dahoun, J. M. Hiver, *Polym. Eng. Sci.* **2011**, *51*, 1607–1616.
[57] R. G. Snyder, J. H. Schachtshneider, *Spectrochim. Acta A* **1964**, *20*, 853–869.
[58] H. Tadokoro, M. Kobayashi, M. Ukita, K. Yasufuku, S. Murahashi, T. Torii, *J. Chem. Phys.* **1965**, *42*, 1432–1448.
[59] G. Zerbi, L. Piseri, *J. Chem. Phys.* **1964**, *49*, 3840.
[60] G. V. Fraser, P. J. Hendra, D. S. Watson, M. J. Gall, H. A. Willis, M. E. A. Cudby, *Spectrochim. Acta A* **1972**, *29*, 1525–1533.
[61] J. M. Chalmers, H. G. M. Edwards, J. S. Lees, D. A. Long, M. W. Mackenzie, H. A. Willis, *J. Raman Spectrosc.* **1991**, *22*, 613–618.
[62] T. C. Damen, S. P. S. Porto, B. Tell, *Phys. Rev.* **1966**, *142*, 570–574.
[63] C. G'Sell, A. Dahoun, V. Favier, J. M. Hiver, M. J. Philippe, G. R. Canova, *Polym. Eng. Sci.* **1997**, *37*, 1702–1711.
[64] R. P. Wool, R. S. Bretzlaff, B. Y. Li, C. H. Wang, R. H. Boyd, *J. Polym. Sci.* **1985**, *24*, 1039–1066.
[65] J. M. Haudin, in Plastic Deformation of Amorphous and Semi Crystalline Materials, (Eds: B. Escaig, C. G'Sell), Les Editions de Physique, Les Ullis, **1982**, pp. 291–311.
[66] M. Aboulfaraj, C. G'Sell, B. Ulrich, A. Dahoun, *Polymer* **1995**, *36*, 731–742.
[67] G. Castelein, G. Coulon, C. G'Sell, *Polym. Eng. Sci.* **1997**, *37*, 1694–1701.
[68] Dijkstra P. T. S., Van Dijk D. J., Huetink J., *Polym. Eng. Sci.* **2002**, *42*, 152–160.
[69] E. Weynant, J. M. Haudin, C. G'Sell, *J. Mater. Sci.* **1980**, *15*, 2677–2692.
[70] E. J. Kramer, in Plastic Deformation of Amorphous and Semi Crystalline Materials, (Eds: B. Escaig, C. G'Sell), Les Editions de Physique, Les Ullis, **1982**, pp. 391-405.